Electronic Supplementary Material (ESI) for Soft Matter.

Electronic Supporting Information

Field driven evaporation kinetics of a sessile ferrofluid droplet on a soft substrate

Sudip Shyam[1], Pranab Kumar Mondal[1*] and Balkrishna Mehta[2]

[1]Microfluidics and Microscale Transport Processes Laboratory , Department of Mechanical Engineering, Indian Institute of Technology Guwahati, Assam 781039, India

[2]Department of Mechanical Engineering, Indian Institute of Technology Bhilai, Raipur 492015, India

Corresponding Author*:- mail2pranab@gmail.com; pranabm@iitg.ac.in

S1. Image processing

A CMOS camera is employed to measure the external hydrodynamics of the ferrofluid droplet. The images are captured at a resolution of 744×480 pixels^2. The captured images are processed further to extract information from it, such as change in contact angle (CA), diameter, height, etc.

a. Determination of CA: The captured side view images are processed in advance ACAM-NSC software to obtain the contact angle. The contact angle(CA) is measured by contour recognition based on the greyscale analysis of the images. The baseline is determined, and the droplet shape was fitted, choosing the more appropriate method. The droplet shape of our sample is determined by three main approaches, namely the tangential(polynomial approximation), young–Laplace, and height–width techniques (where the profile was found as a part of a circle enclosed in a rectangle). The contact angle was found by fitting a tangent to the shape of the contact line. The mean between the two measured contact angle (left and right) is taken. The accuracy of the contact angle measurements was around $\pm0.3^{\circ}$.

b. Determination of diameter, height, and contact line velocity of the droplet. Unsharp masking is carried out on the captured droplet images employing imageJ[1] software. The unsharp masking algorithm ensures a sharpening of the droplet images. The sharpened images are converted to a 8-bit binary image. The binary image typically contains pixels intensity values as either '0' or '255'. The images are then outlined i.e. only the edges are detected. Following this, the pixels information of the images is fed to the in-house developed code for determining the respective temporal changes in height, diameter, and contact line velocity of the droplet. In Fig. S1, we show schematic of all the sequence of the involved image processing.

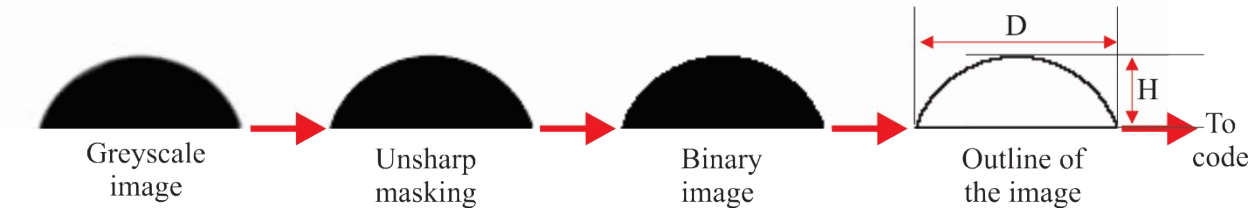

Fig. S1 (Color online) The plot illustrates the sequence of the image processing steps involved for extracting information such as diameter, height, contact line velocity, from the droplet images.

S2. Distribution of magnetic field

The magnetic field distribution is numerically simulated with COMSOL® Multiphysics for the given physical situation. In the present study, only the magnetic field distribution is solved numerically, while the hydrodynamics inside the droplet is quantified only experimentally as already mentioned by using μ-PIV. To obtain the magnetic field inside the droplet, the following equations are solved: Ampere's law: $\overline{\nabla} \times \overline{\mathrm{H}} = \overline{\mathrm{J}}$, where $\overline{\mathrm{H}}$ is the magnetic field intensity, $\overline{\mathrm{J}}$ is the current density and given by, $\overline{\mathrm{J}} = \sigma\left(\overline{u}_c \times \overline{\mathrm{B}}\right) + \overline{\mathrm{J}}_e$, where $\overline{u}_c$ is the velocity of the conductor and $\overline{\mathrm{J}}_e$ is the externally generated current density. Note that this externally generated current density is given by $\overline{\mathrm{J}}_e = \left(\mathrm{N}\overline{\mathrm{I}}/a_{coil}\right)$, where N, is the number of turns, $\overline{\mathrm{I}}$ is the supplied current, and a_{coil} is the cross-sectional area of the wire. Now, using magnetic vector potential $\overline{\mathrm{A}}_m$, we can write the magnetic field flux as $\overline{\mathrm{B}} = \nabla \times \overline{\mathrm{A}}_m$. Note that employing the constitutive relationship $\overline{\mathrm{B}} = \mu_0\left(\overline{\mathrm{H}} + \overline{\mathrm{M}}\right)$; where $\overline{\mathrm{M}}$ is the magnetization, Ampere's law can be rewritten as: $\sigma\left(\partial \overline{\mathrm{A}}_m/\partial t\right) + \nabla \times \left(\mu_0^{-1} \cdot \mu_r^{-1} \cdot \overline{\mathrm{B}}\right) - \sigma \overline{u}_c \times \overline{\mathrm{B}} = \overline{\mathrm{J}}_e$. The permeability of the vacuum and the relative permeability are expressed by μ_0 and μ_r respectively. While solving the equations, we used the tangential component of the magnetic potential $\left(\mathbf{n} \times \overline{\mathrm{A}}_m = 0\right)$ as zero (equivalent to magnetically insulating the computational domain) at the boundary of the domain. The parametric values considered for the present computations are as follows: $\overline{\mathrm{I}} = 1.5\,\mathrm{A}$, $a_{coil} = 2.82 \times 10^{-5}\,\mathrm{m}^2$ $\mu_0 = 1.257 \times 10^{-6}\,\mathrm{H/m}$ (Henry/meter), $\mu_r = 1$ and N=800.

In Fig. S2(a), we show the distribution of the magnetic field around the droplet domain. Quite intuitively, it can be observed from Fig. S2(a) that as one move away from the magnet, the magnetic field strength decreases. Figure S2(b) depicts the variation of the magnetic field flux (B) along the line of symmetry XX' and YY'. The droplet region experiences a drop of around 200G in the magnetic field flux along the line XX'. While along the YY' line, the magnetic field strength is almost constant. The high gradient of magnetic field flux along the XX' line of symmetry as compared to YY' direction ensures that the sole effect of the magnetic field will be to retain the MNP's at the magnetically active zone (near the liquid-air interface of the active magnet).

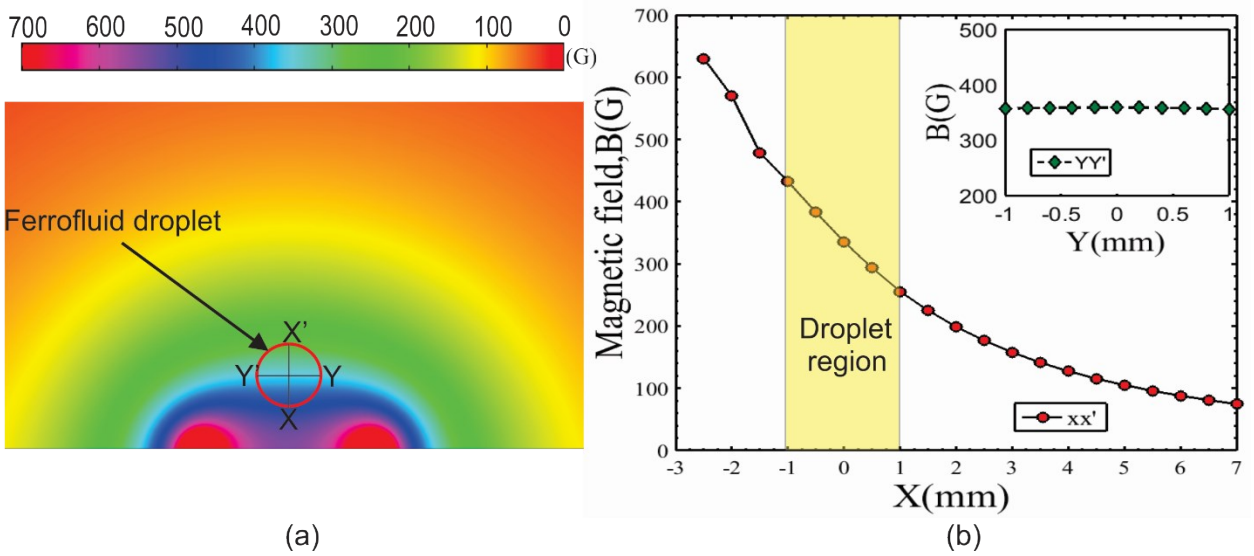

Fig. S2 (Color online) (a) The plot shows the distribution of magnetic flux density $(\vec{B})$ around the droplet region. The red circle denotes the ferrofluid droplet. $X-X'$ and $Y-Y'$ indicates the symmetric lines inside the ferrofluid droplet domain. (b) Plot depicts the variation of magnetic flux density $(\vec{B})$ along the $X-X'$ line of symmetry of the droplet. The yellow marked region denotes the droplet flow field. The inset shows the magnetic flux density variation along the Y-Y´. The position $X=0, Y=0$ signifies the center of the droplet.

S3 Validation

Figure S3 validates the μ-PIV technique with the experimental result of Saroj and Panigrahi[2], in the absence of an external magnetic field. A good match between the two velocity profiles along the YY' line, benchmarks the adopted μ-PIV technique. This validation further justifies the credibility of the observation that seeding particles follow the direction of bulk flow with negligible interference from nanoparticles in the absence of any external force.

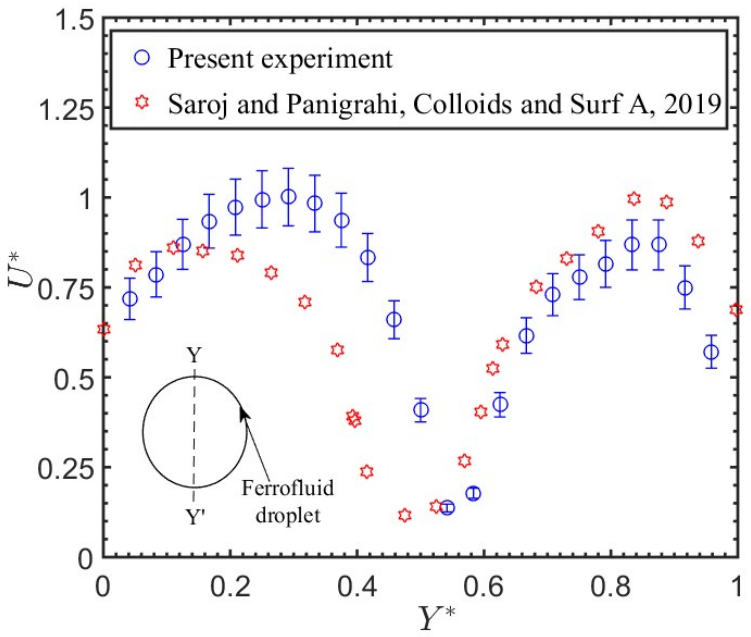

Fig. S3: Validation of the adopted μ-PIV technique with the result of Saroj and Panigrahi.[2] Inset depicts the schematic of the droplet indicating the YY' line of symmetry along which the velocity profile is calculated. $U^* = u/u_{\max}$, where $u_{\max}$, is the maximum velocity and $Y^* = y/D$, where D, is the diameter of the droplet.

S4 Scaling analysis

To explore the interactions between the seeded fluorescent particles and the magnetic nanoparticles during the μ-PIV measurement, a scaling analysis is carried out. The primary role of the scaling analysis is to quantify the presence of negative magnetophoresis occurring in the droplet domain. The negative magnetophoresis is the phenomenon that is usually encountered by a non-magnetic body like seeding particles dispersed in a magnetic medium like ferrofluid in the presence of a magnetic field.[3,4] The deflection of non-magnetic particles due to negative magnetophoresis can be minimized with the use of diluted ferrofluid and a low strength of the applied magnetic field.[5] The negative magnetophoretic force (F_{mp}) and viscous drag force (F_d) acting on seeding particles under the present experimental conditions were calculated and the ratio between the two was found to be $(F_{mp}/F_D) \sim 10^{-4}$. This low value of F_{mp}/F_D indicates negligible influence of negative magnetophoresis and the domination of the drag force on the motion of the seeded particles. Consequently, we observe the seeding particles to follow the bulk

flow motion faithfully inside the droplet in the presence of a magnetic field during the μ-PIV measurements.[6]

Supporting Videos

S1 The video shows the motion of the magnetic nanoparticle's (MNP's) inside the ferrofluid droplet domain under the influence of the time-dependent magnetic field. The electromagnet perturbs the droplet flow domain at f=0.5 Hz. The video speed is made faster by 0.1x.

S2 The video shows the motion of the magnetic nanoparticle's (MNP's) inside the ferrofluid droplet domain under the influence of the time-dependent magnetic field. The electromagnet perturbs the droplet flow domain at f=1 Hz. The video speed is made faster by 0.1x.

S3 The video shows the motion of the magnetic nanoparticle's (MNP's) inside the ferrofluid droplet domain under the influence of the time-dependent magnetic field. The electromagnet perturbs the droplet flow domain at f=3 Hz. The video speed is made faster by 0.1x.

References

1 C. A. Schneider, W. S. Rasband and K. W. Eliceiri, *Nat. Methods*, 2012, **9**, 671–675.

2 S. K. Saroj and P. K. Panigrahi, *Colloids Surfaces A Physicochem. Eng. Asp.*, 2019, **580**, 123672.

3 G.-P. Zhu, M. Hejiazan, X. Huang and N.-T. Nguyen, *Lab Chip*, 2014, **14**, 4609–4615.

4 L. Liang, C. Zhang and X. Xuan, *Appl. Phys. Lett.*, 2013, **102**, 234101.

5 T. Zhu, D. J. Lichlyter, M. A. Haidekker and L. Mao, *Microfluid. Nanofluidics*, 2011, **10**, 1233–1245.

6 S. Shyam, M. Asfer, B. Mehta, P. K. Mondal and Z. A. Almutairi, *Colloids Surfaces A Physicochem. Eng. Asp.*, 2019, 124116.